

Numerical Investigations on behavior of a modified simple hypoplastic model by using finite elements

Sendy F Tanton¹

¹Civil Engineering Department, Widya Karya Catholic University

Korespondensi Penulis: sendyantono@widyakarya.ac.id

(Received 1 Des 2024; Revised 8 Des 2024; Accepted 16 Des 2024)

Abstract

This short study describes about the behavior of a simple hypoplastic equation proposed by Wu Wei (1992) with applying modified stress update algorithm routine. Details of the model and the modified algorithm are described in Section 2. Motivation of this modification is to have a more stable solution algorithm than original one. The “more stable solution” here means only homogeneous deformation may occur during oedometric and plane strain compression test on single element. The inhomogeneous deformation of single element might be triggered by the evolution of shear stress. In the Sections 3 the finite element modeling of oedometric and plain strain compression test is described, followed by the comparison of the result of modified and original algorithm routine. In addition, the simulation of the penetration of footing into sand specimen is also simulated by applying the modified algorithm routine on the hypoplastic model. The result is compared with those using elasto-plastic Drucker Prager model.

Keywords: hypoplastic, algorithm, stable solution, deformation.

1. Introduction

Theory of Hypoplasticity has been developed by Kolymbas and Gudehus and their associates since late seventies (Kolymbas, 1991, Kolymbas & Wu, 1993, Niemunis, 1993, Wu & Bauer, 1994). Hypoplastic models have been shown to perform well for deformations due to rearrangements of the grain skeleton. However, in the application of hypoplastic constitutive equation to the finite element modeling, one may face instability calculation such as inhomogeneous deformation of single element which might be triggered by evolution of shear stress. The modified algorithm routine is introduced to obtained “more stable” solution. Finite element model of oedometric test and plane strain test are given. Finally, the simulation of footing penetration into sand specimen is shown.

2. Hypoplastic model

In the hypoplastic model, the stress increment equation is described by a constitutive equation of rate type which is decomposed into linear and nonlinear in strain rate tensor

$$\dot{\mathbf{T}}_{ij} = \mathbf{L}_{ijkl} : \mathbf{D}_{kl} + \mathbf{N}_{ij} \|\mathbf{D}_{kl}\| \quad (1)$$

with $\dot{\mathbf{T}}$ the Jaumann stress rate and \mathbf{D} strain rate. The colon $:$ denotes inner product between two tensors and $\|\mathbf{D}\| = \sqrt{\mathbf{D} : \mathbf{D}}$. In this study, the specific representation of hypoplastic model proposed by Wu Wei (1992) is used and read as

$$\dot{\mathbf{T}}_{ij} = C_1 (\text{tr } \mathbf{T}) \mathbf{J}_{ijkl} \mathbf{D}_{kl} + C_2 \frac{(\mathbf{T}_{kl} : \mathbf{D}_{kl})}{\text{tr } \mathbf{T}} \mathbf{T}_{ij} + C_3 \frac{\mathbf{T}_{ij} \mathbf{T}_{ij}}{\text{tr } \mathbf{T}} \|\mathbf{D}_{kl}\| + C_4 \frac{\mathbf{T}_{ij}^d \mathbf{T}_{ij}^d}{\text{tr } \mathbf{T}} \|\mathbf{D}_{kl}\|, \quad (2)$$

where C_i ($i = 1, \dots, 4$) are dimensionless parameter, \mathbf{J}_{ijkl} is described by $\mathbf{J}_{ijkl} = \delta_{ik} \delta_{jl}$. In Eq. 2 the deviatoric stress tensor is given by $\mathbf{T}_{ij}^d = \mathbf{T}_{ij} - 1/3 * (\text{tr } \mathbf{T}) \mathbf{1}$.

Since the material behavior is rate independent a fictitious time scale can be introduced for a quasi-static loading process. A loading stress is divided into increments, which corresponds to a division of a prescribed time domain into time increments. Once the displacement increment is obtained, the stress can be updated by using the implicit integration formulation. The unknown stress at time $t = n+1$ can be determined as

$$\mathbf{T}_{t=n+1} = \mathbf{T}_{t=n} + \Delta \mathbf{T}. \quad (3)$$

where $\Delta \mathbf{T}$ is the stress increment equation calculated from Eq. 2. In addition, the modification of stress increment $\Delta \mathbf{T}$ is shown in Eq. 6. Here, Taylor expansion is introduced in the linear and nonlinear part of Eq. 1 as

$$\mathbf{L}_{ijkl}^{n+\theta} = \mathbf{L}_{ijkl}^n + \theta \frac{\partial \mathbf{L}_{ijkl}^n}{\partial \mathbf{T}_{ab}} : \Delta \mathbf{T}_{ab} \quad \text{and} \quad (4)$$

$$\mathbf{N}_{ij}^{n+\theta} = \mathbf{N}_{ij}^n + \theta \frac{\partial \mathbf{N}_{ij}^n}{\partial \mathbf{T}_{ab}} : \Delta \mathbf{T}_{ab}, \quad (5)$$

where θ is interpolation parameter and for stability $\theta > 0.5$. By taking $\theta = 1.0$ and substituting Eqs. 4 & 5 into Eq. 1, stress increment $\Delta \mathbf{T}$ in Eq. 3 reads as

$$\Delta \mathbf{T}_{ab} = \left[\mathbf{J}_{ijab} - \left(\frac{d\mathbf{L}_{ijkl}}{d\mathbf{T}_{ab}} \right) : \mathbf{D}_{kl} * \Delta t - \left(\frac{d\mathbf{N}_{ij}}{d\mathbf{T}_{ab}} \right) \|\mathbf{D}\| * \Delta t \right]^{-1} * \left(\mathbf{L}_{ijkl} : \mathbf{D}_{kl} * \Delta t + \mathbf{N}_{ij} \|\mathbf{D}\| * \Delta t \right) \quad (6)$$

(6)

with $\mathbf{J}_{ijkl} = \delta_{ik} \delta_{jl}$.

The stiffness matrix \mathbf{K}_{ij} can be described from implicit function, reads

$$\mathbf{F} \equiv -\Delta \mathbf{T}_{ij} + \mathbf{L}_{ijkl} : \mathbf{D}_{kl} * \Delta t + \mathbf{N}_{ij} \|\mathbf{D}\| * \Delta t + \left(\left(\frac{d\mathbf{L}_{ijkl}}{d\mathbf{T}_{ab}} \right) : \mathbf{D}_{kl} * \Delta t \right) : \Delta \mathbf{T}_{ab} + \theta * \left(\left(\frac{d\mathbf{N}_{ij}}{d\mathbf{T}_{ab}} \right) \|\mathbf{D}\| * \Delta t \right) : \Delta \mathbf{T}_{ab} = \mathbf{0} \quad (7)$$

and

$$\mathbf{K} = - \frac{\partial \mathbf{F} / \partial (\mathbf{D}_{kl} \Delta t)}{\partial \mathbf{F} / \partial (\Delta \mathbf{T}_{ab})}$$

For the nonsymmetric matrix, the stable condition of critical state could be maintained by checking the positiveness of all eigen-values of matrix $\mathbf{K}_{new} = 0.5 * (\mathbf{K} + \mathbf{K}^T)$, not of matrix \mathbf{K} (de Borst, 1986). In order to check the positiveness of eigen-values, Bromwich (1906) stated that every eigen-value of nonsymmetric matrix satisfies:

$$\hat{\lambda}_1 \leq \text{Re } \lambda \leq \hat{\lambda}_n$$

where $\hat{\lambda}_1$ and $\hat{\lambda}_n$ are the smallest and largest eigen-values, respectively. Therefore by only checking the positiveness of smallest eigen-value of \mathbf{K}_{new} , the stability of critical state is obtained (Bazant & Cedolin, 2003).

The detail algorithm is drawn in the flowchart shown in Fig.1

3. Finite element Calculation

In this finite element calculation by Abaqus ver.6.3, there are three tests are simulated, namely oedometric compression test, plane strain compression test, and penetration of footing into sand specimen. For oedometric test and plane strain compression test, the simulations are carried out by using single element and discrete structure. In all simulations, a four nodes linear element is used. The comparison results between using original algorithm and modified algorithm described above are shown. Incase of the simulation of footing penetration, only the result by modified algorithm is shown and compared with those simulation by using elasto-plastic Drucker Prager model.

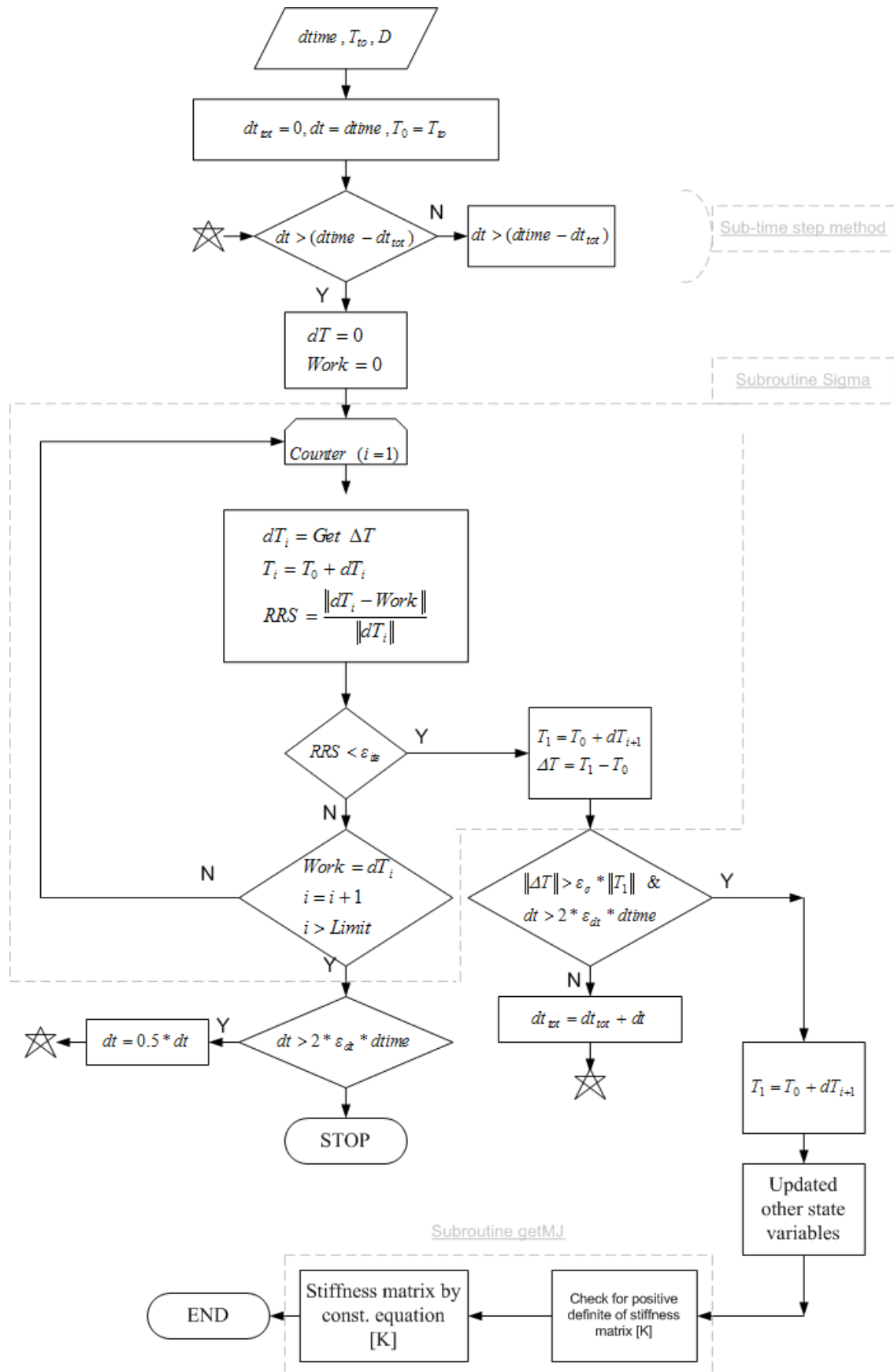


Fig. 1 Flow chart of the time integration scheme

In these simulations, a nonlinear geometry analysis is applied, as consequences, local instabilities problem might occur due to local transfer of energy between elements. This can be solved by introducing artificial mass matrix with damping factors into general nonlinear equilibrium equation, $P_{ex} - P_{in} - c * M * v = 0$, where P_{ex} and P_{in} are external and internal force; M , v and c are artificial mass matrix calculated with unity density, nodal velocity and damping factor, respectively. It is worth to note that in Abaqus program, this artificial damping factor can be applied by using stabilize option.

The material constants of dense and loose Karlsruhe sand used in the simulation are summarized in table below (Wu & Bauer, 1994):

Karlsruhe sand	C_1	C_2	C_3	C_4
Dense	-101.2	-962.1	-877.3	1229.2
Loose	-69.4	-673.1	-655.9	699.6

4. Results and Discussions

4.1 Oedometric test

4.1.1 Modeling

Dimension of the specimen is $4 \times 4 \text{ cm}^2$. Fig 2 shows boundary condition used in the oedometric test of single element.

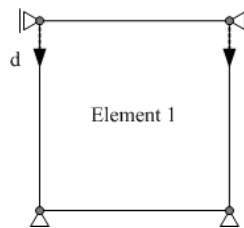


Fig. 2 Illustration of the simulation oedometric test

The procedure is described as the following:

- equilibrium of initial isotropic compression of 100 kPa is applied,
- downward vertical displacement of -0.2 cm is prescribed at top node of the specimen, unloading the vertical displacement up to -0.05 cm measured from the initial position.

4.1.2 Results

Results of the simulation of oedometric test using single element are shown in Figs 3-5. In particular, Figs 3(a) & (b) show the normalized vertical (S_{22}/S_{11}) and shear stress (S_{12}/S_{11}) of dense and loose sand due to loading of -0.2 cm and unloading up to -0.05 cm. The value of normalized shear stress is very small ($< 10^{-17}$), which means that only homogeneous deformation occurs. However, a problem occurred when large loading - unloading of vertical displacement of -0.8 cm and 0.8 cm is applied on top of specimen. The calculation of original model failed before unloading step started. This might be happened because the element is no longer homogeneous where the shear stress increases very fast. By using a modification which is described in Section 2, a more stable result can be obtained, in the sense that the deformation of single element test is in homogeneous shape. The comparison results between applying original and modified algorithm version on the oedometric simulation with loading - unloading vertical displacement of -0.8 - 0.8 cm are shown in Fig 4(a) & (b) for normalized vertical stress and normalized shear stress, respectively. The evolution of coefficient earth pressures K_0 of dense sand and loose sand is shown in Fig 5. In loading condition, they are 0.487 and 0.521 for dense and loose sand. Nonlinear behavior of K_0 is clearly observed when un-loading condition is applied.

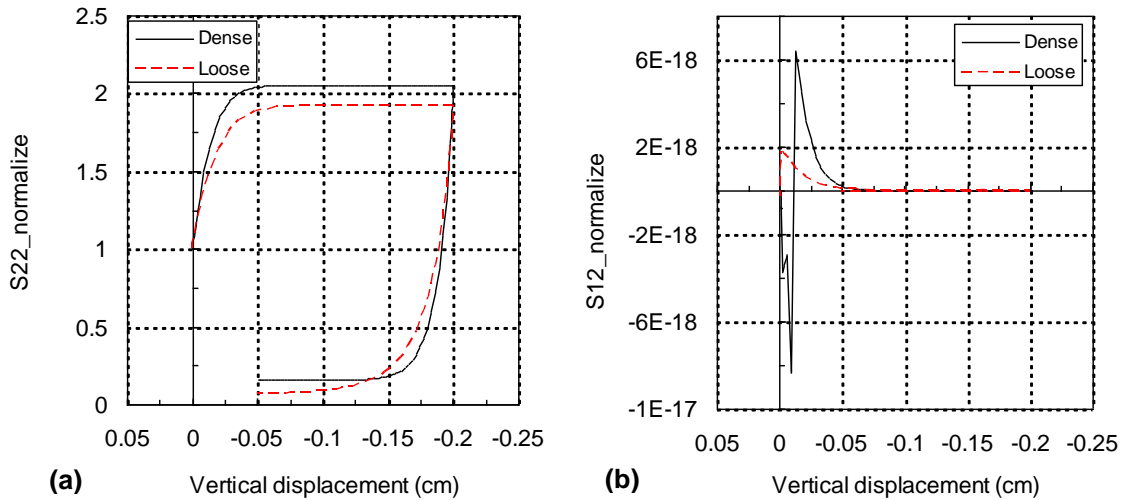


Fig. 3 Evolution of normalized (a) vertical stress, (b) shear stress during loading/unloading

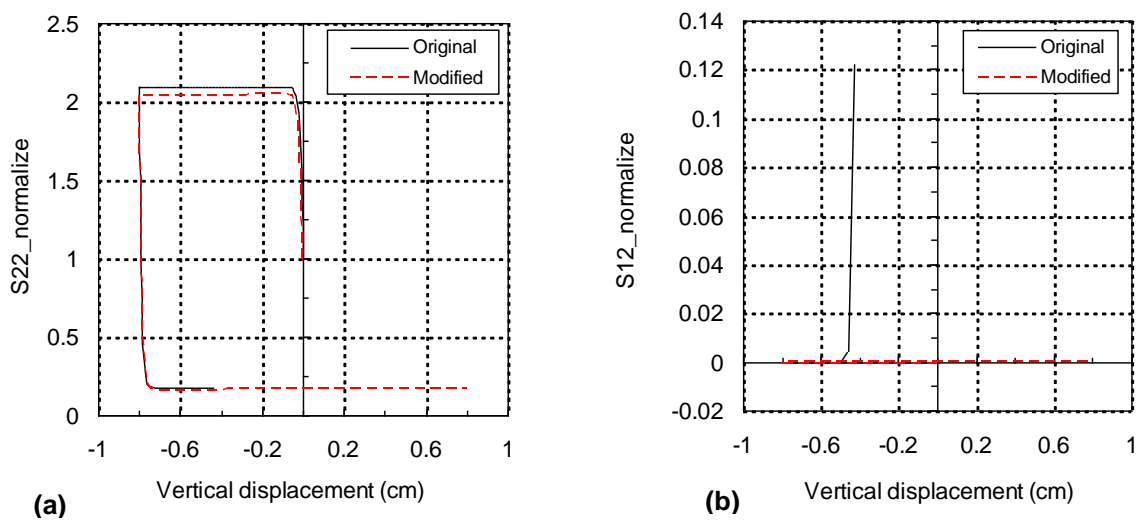


Fig. 4 Comparison between original model and modified model during large loading/unloading: evolution of normalized (a) vertical stress, (b) shear stress

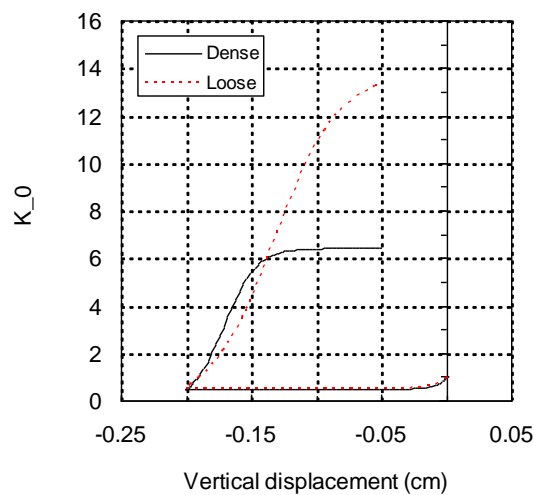


Fig. 5 Evolution of coefficient of earth pressure at rest K_0 under loading-unloading for dense and loose sand

In addition to single element, the behavior of discrete element (4 x 4 elements) of 4 x 4 cm² under loading and unloading condition is also investigated. The procedure is the same as that is used for single element. The results show that the behavior of normalized vertical stress is the same that of single element (Fig. 6). Fig. 7 shows the evolution of shear stress during loading and unloading. It is clear that during loading no shear stress develops while after certain unloading of vertical displacement the shear stress starts to develop to small values compared to that of horizontal stress.

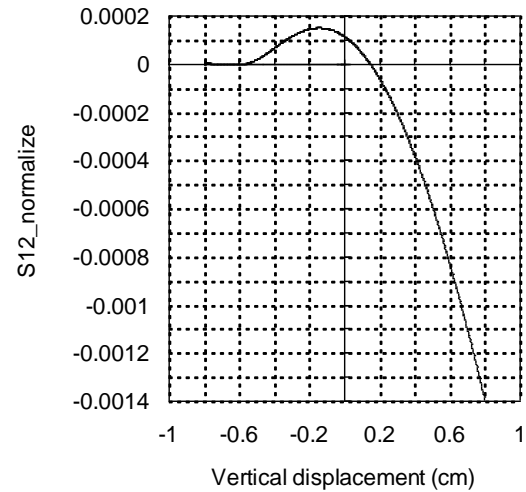
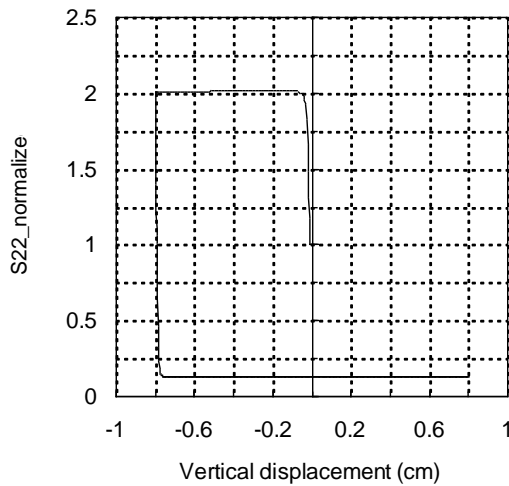


Fig. 6 Evolution of normalized vertical stress Fig. 7 Evolution of normalized shear stress

4.2 Plane strain compression test

4.2.1 Modeling

Here, the plane strain compression test is simulated as single element and discrete elements. The simulation of single element is conducted by using the same element size as that used in oedometric compression test while 4 x 8 cm² specimen is simulated by using 8 x 16 discrete elements. The procedure of loading is similar to that of for oedometric compression; after applying initial isotropic stress of 100 kPa, downward vertical displacement of 0.0036 m is prescribed on top of specimen with single element and that of vertical displacement of 2 cm is used for discrete element.

During the application of this displacement loading the lateral pressure H of 100 kPa is constantly applied on the right side of element. The boundary conditions used in plane strain compression test are shown in Fig 8.

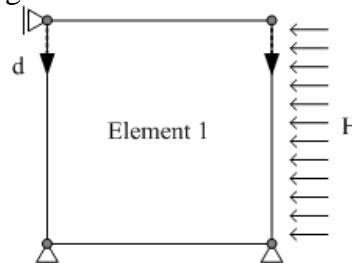


Fig. 8 Illustration of the simulation of plane strain compression test

4.2.2 Results

In the single element test, the original model seems to work well for dense and loose specimens. The dilatancy behavior of dense sand, as well as compaction behavior of loose sand can be smoothly modeled as shown in Fig 9. The stress ratio of dense sand is stiffer and higher than that of loose sand (Fig. 10). However, similar to the inhomogeneity problem faced in the simulation of oedometric compression, the original model shows anomaly behavior when

loading of vertical displacement higher than 0.0036 cm is applied, as shown in Fig 11. It can be observed that the evolution of horizontal displacement of Node1 and Node2 is slightly different. This inhomogeneity is clearly shown in the evolution of normalized shear stress S_{12}/S_{11} , volumetric strain and stress ratio S_{22}/S_{11} (Figs. 12-14). In particular, the normalized shear stress behavior (Fig. 12) suddenly increases at about vertical strain of -0.09 while a sudden drawdown of stress ratio (Fig. 14) is also observed at about the same vertical strain.

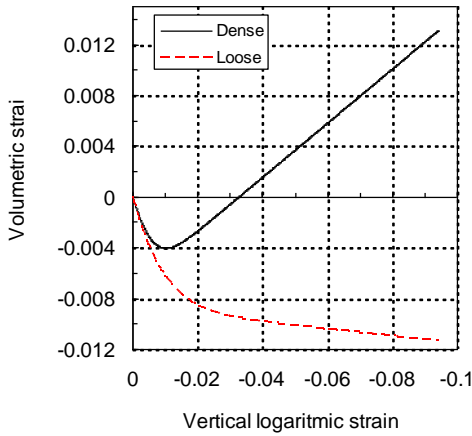


Fig. 9 Evolution of volumetric strain

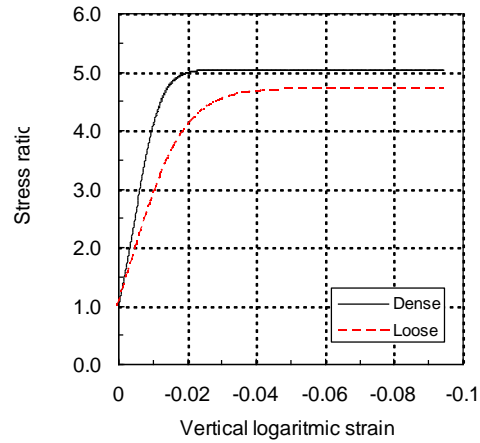


Fig. 10 Evolution of stress ratio

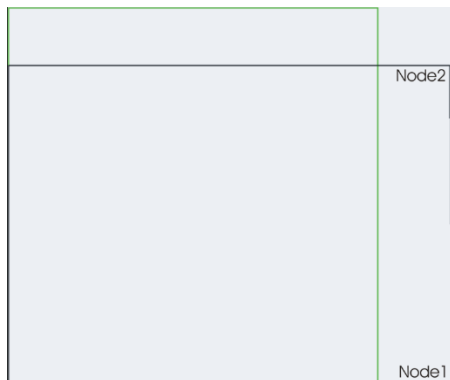


Fig. 11 Deform shape - Original algorithm

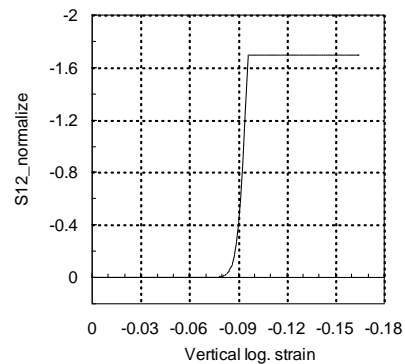


Fig. 12 Evolution of S_{12} / S_{11}

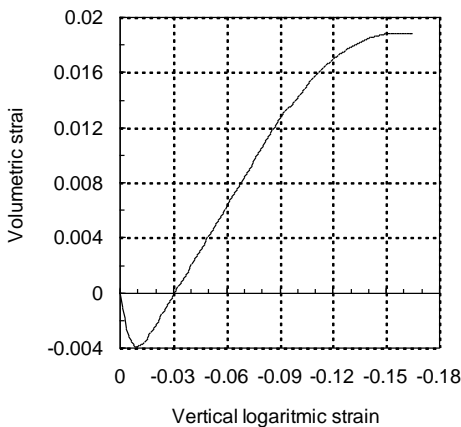


Fig. 13 Evolution of volumetric strain

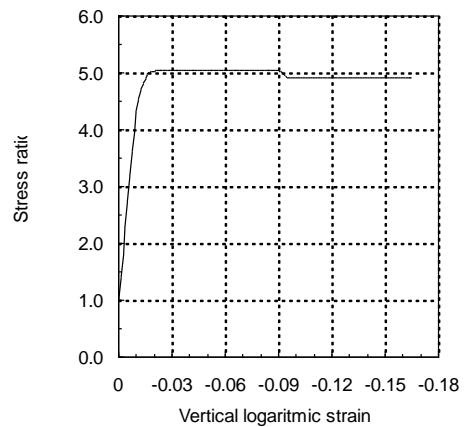


Fig. 14 Evolution of stress ratio

This inhomogeneity cannot be true since it is occurred in the single element test. Therefore, a modified algorithm described in Section 2 is needed. The results after using modified algorithm are shown in Figs. 15-18. Homogeneous deformation can be directly observed from the deform

shape and evolution of normalized shear stress, as shown in Figs. 15 & 16. The normalized shear stress fluctuates in only very small values. The dilatancy behavior, as well as the stress ratio evolution of dense specimen under loading-unloading-reloading can also be smoothly captured, as shown in Figs 17 & 18.



Fig. 15 Deform shape – Modified algorithm

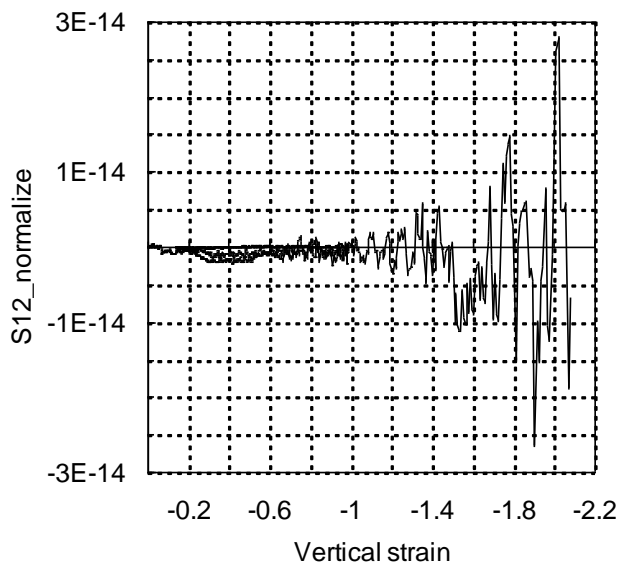


Fig. 16 Evolution of S_{12} / S_{11}

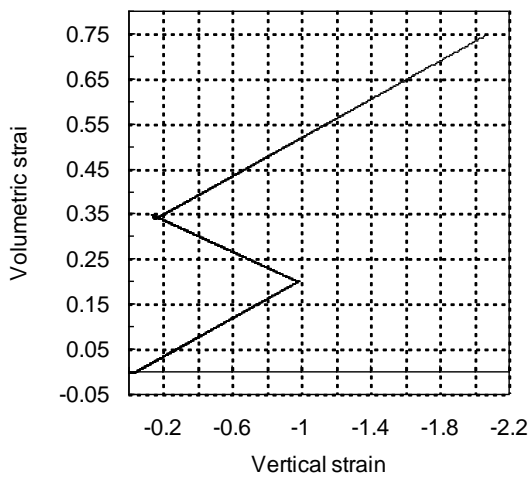


Fig. 17 Evolution of volumetric strain

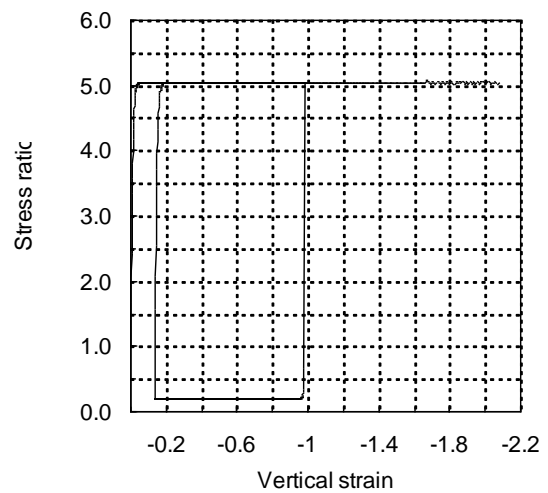


Fig. 18 Evolution of stress ratio

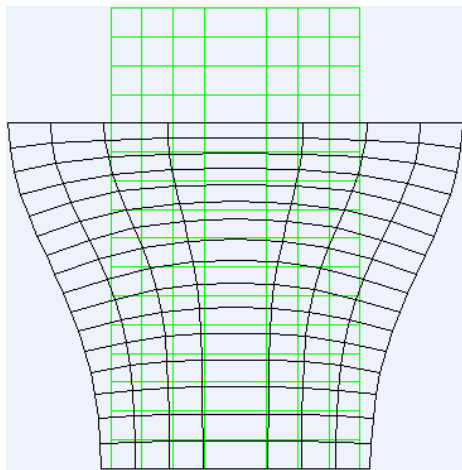


Fig. 19 Deform shape – Modified algorithm

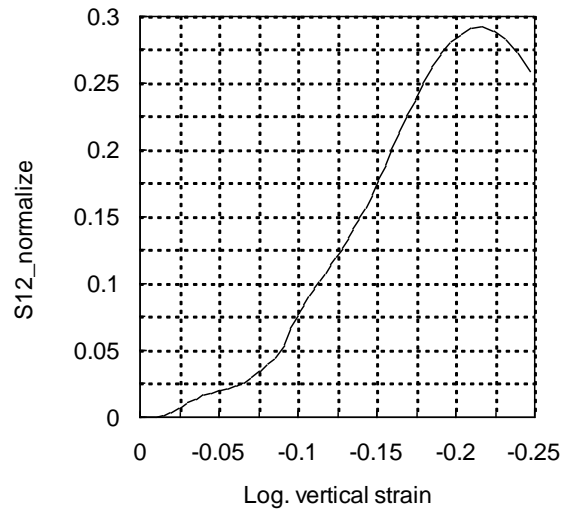


Fig. 20 Evolution of S_{12} / S_{11}

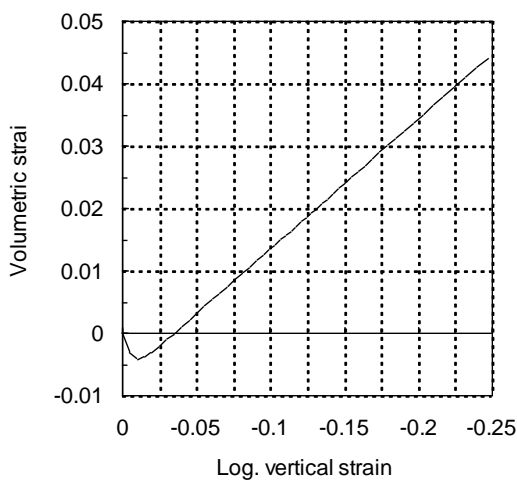


Fig. 21 Evolution of volumetric strain

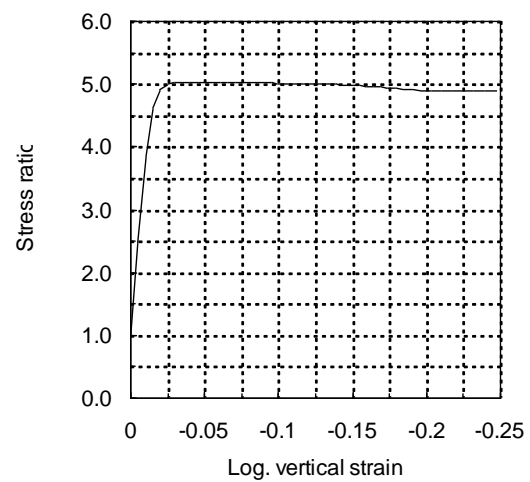
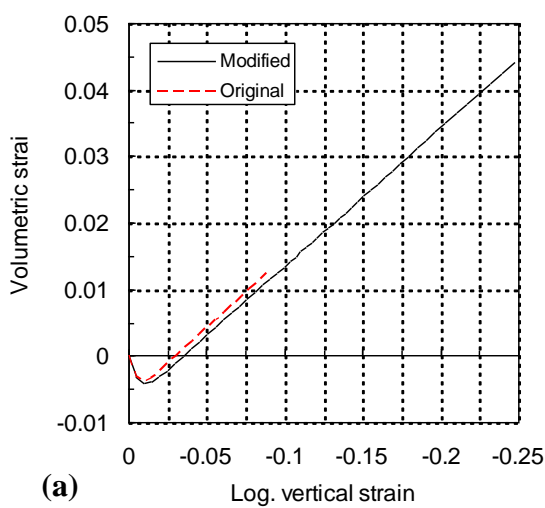
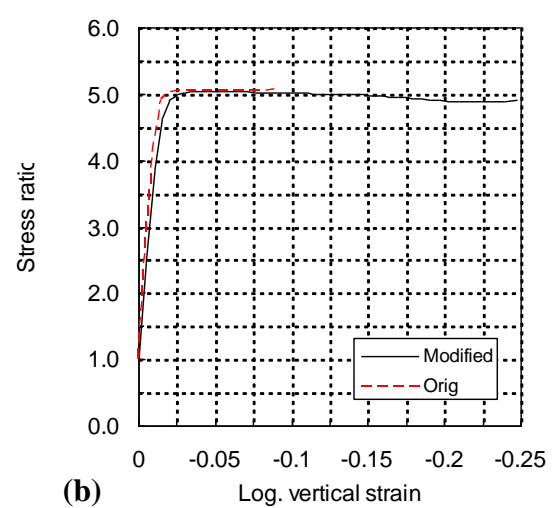


Fig. 22 Evolution of stress ratio



(a)



(b)

Fig. 23 Comparison between original and modified algorithm for
 (a) Volumetric strain, (b) stress ratio

In addition to the simulation of single element, the plane strain compression test is also simulated by using discrete elements, applying both types of stress update algorithms. By using modified algorithm, the calculation result shows inhomogeneity of the deformation shape after vertical displacement of 2 cm (Fig. 19). The corresponding evolution of normalized shear stress, volumetric strain and stress ratio at the middle element are shown in Figs. 20-22. Here, the effect of inhomogeneity deformation is clearly shown by sudden decreased of stress ratio (Fig. 22). Comparing the original and modified algorithm, the initial compression can be smoothly captured by both algorithms; however, the dilatancy behavior of specimen cannot be shown smoothly by original one. The unsuccessful calculation due to convergence problem is shown after certain vertical displacement (Figs. 23 (a) & (b)).

4.3 Penetration of footing into sand specimen

4.3.1 Modeling

A 400 x 100 cm² box of soil specimen is also modeled by 48 x 40 four nodes linear elements while the footing is illustrated as a prescribed vertical displacement of 21.75 cm applied along 40 cm at the middle of soil box. The initial gravity loading of 2.0t/m³ is used before the footing penetrates the soil box and a vertical pressure of 1 kPa is applied on top surface of soil box. Since the footing is placed in the middle of soil box the problem may be considered in symmetry condition. It is worth to note that the smaller element size is used near the footing corner and the further the distance from footing the larger element size which is used, as shown in Fig. 24. In this simulation, the interface between footing and soil is assumed to be very rough so that no relative displacement is allowed between sand particle and footing surface. Here, two constitutive models are used and compared, namely hypoplastic model with modified algorithm (described in Section 2) and elasto-plastic Drucker Prager model. Parameter constants used in hypoplastic model is the same that used in oedometric and plane strain compression simulation while those used in elasto-plastic Drucker Prager model are chosen by fitting the results of the simulation of plane strain compression test done by hypoplastic model with modified algorithm (Figs. 25-26). The parameter constants resulted from curve-fitting are as follows

Elastic mod. (kPa)	Poisson ratio	Friction angle (deg.)	Dilation angle (deg.)	τ at $\sigma_N = 0$ (kPa)	K_{ratio}
3.036E+4	0.328	30	10	120	1.0

with K_{ratio} is a constant related to the shape of yield surface at the deviatoric plane; $K=1.0$ is circle.

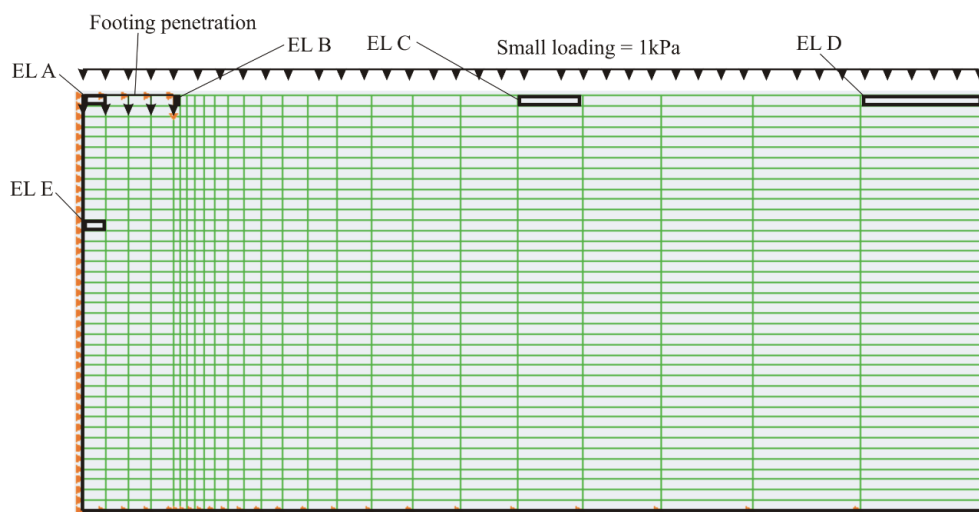


Fig. 24 Illustration of footing penetration into sand specimen

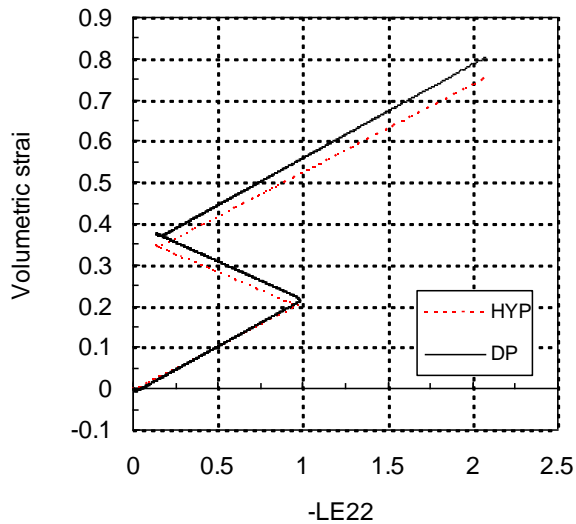


Fig. 25 Evolution of volumetric strain

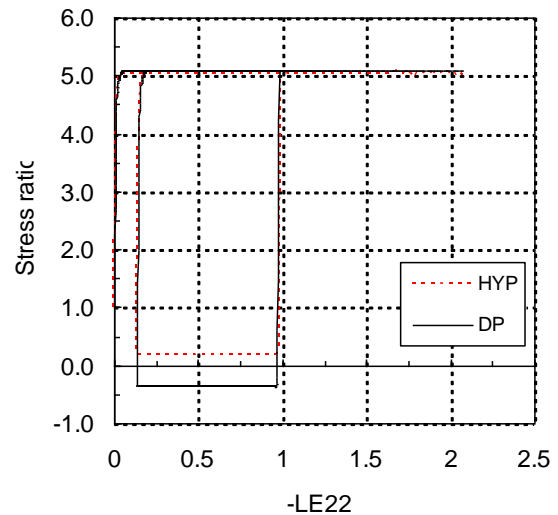


Fig. 26 Evolution of stress ratio

The results of the simulation show that in both models heaving of top surface soil specimen can be observed at the certain distance from the corner of the footing (Figs. 27 & 28). For the element EL A, Drucker Prager model give higher degree of compression, approximately twice of that by hypoplastic model (Fig. 29(a)) while the dilatancy behavior of the element at element EL B can be captured by hypoplastic model and the degree of dilatancy is only slightly different compared to that of by Drucker Prager model (Fig. 29 (b)). Here, the evolution of dilatancy behavior by Drucker Prager goes to the very high value. It should be noted that the oscillation behavior shown by Drucker Prager model (Fig. 29(b)) is due to the distortion of the element (see Fig. 28).

Fig. 30 shows the volumetric behavior of the soil around the footing after penetration of 21.75 cm when the hypoplastic model is used. Here, the black color shows compression behavior (sign: negative). It shows that this contour of dilatancy behavior have a similar tendency as those shown by Prandtl mechanism. Detail dilatancy/compression behavior of element EL C, D, and E are shown in Fig. 31(a). It is also observed that the dilatancy behavior by elastoplastic Drucker Prager model is not too pronounced compared to hypoplastic model as shown in Fig. 31(b).

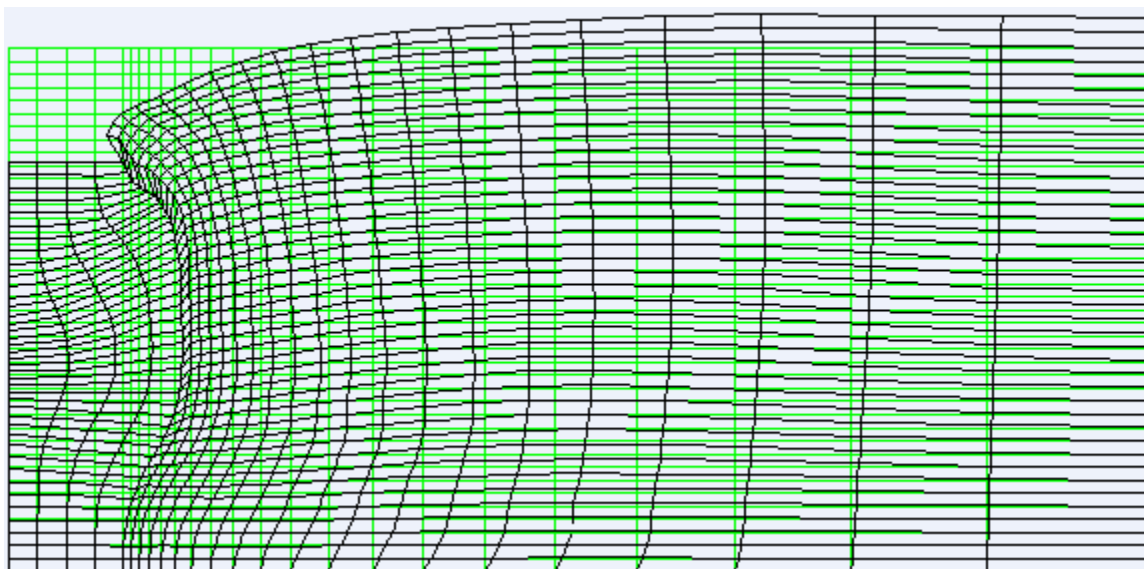


Fig. 27 Deform shape of the soil specimen due to footing penetration --- hypoplastic model

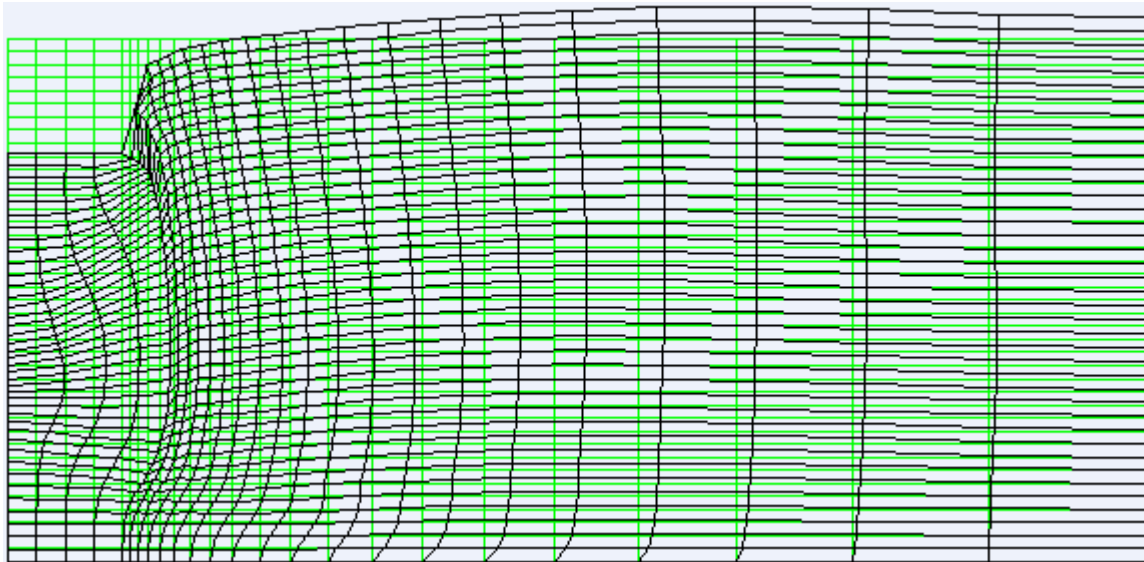


Fig. 28 Deform shape of the soil specimen due to footing penetration --- Drucker Prager model

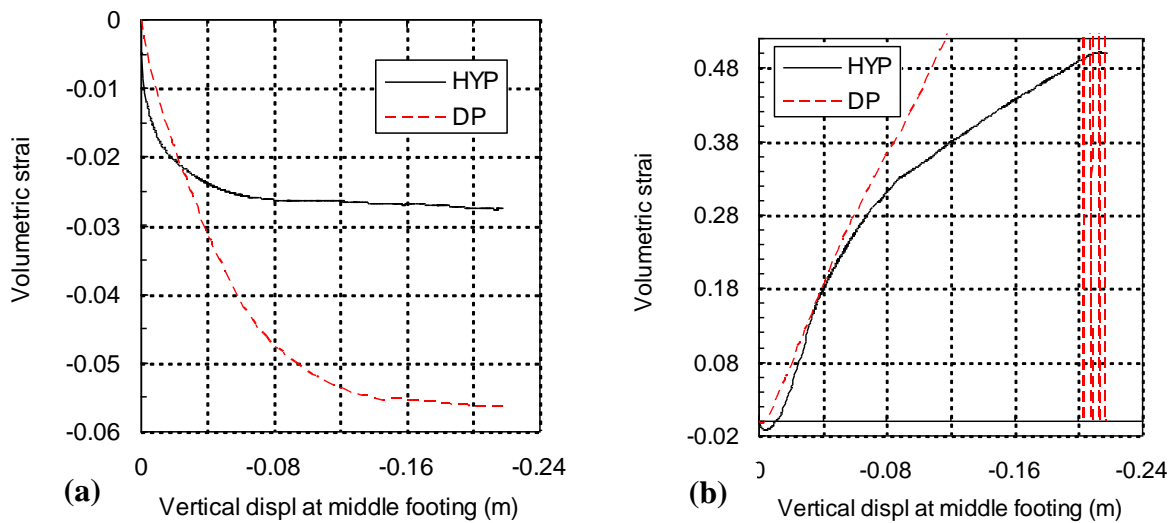


Fig. 29 Comparison between hypoelastic model and elasto-plastic Drucker Prager model for volumetric behavior of element (a) below, (b) at the corner of the footing

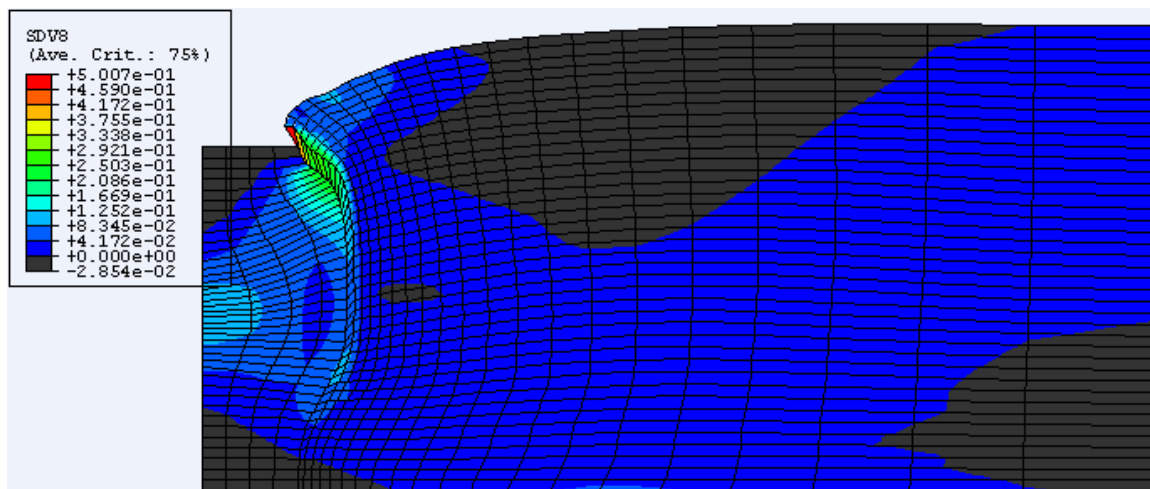


Fig. 30 Volumetric behavior of soil around footing after penetration of 21.75 cm

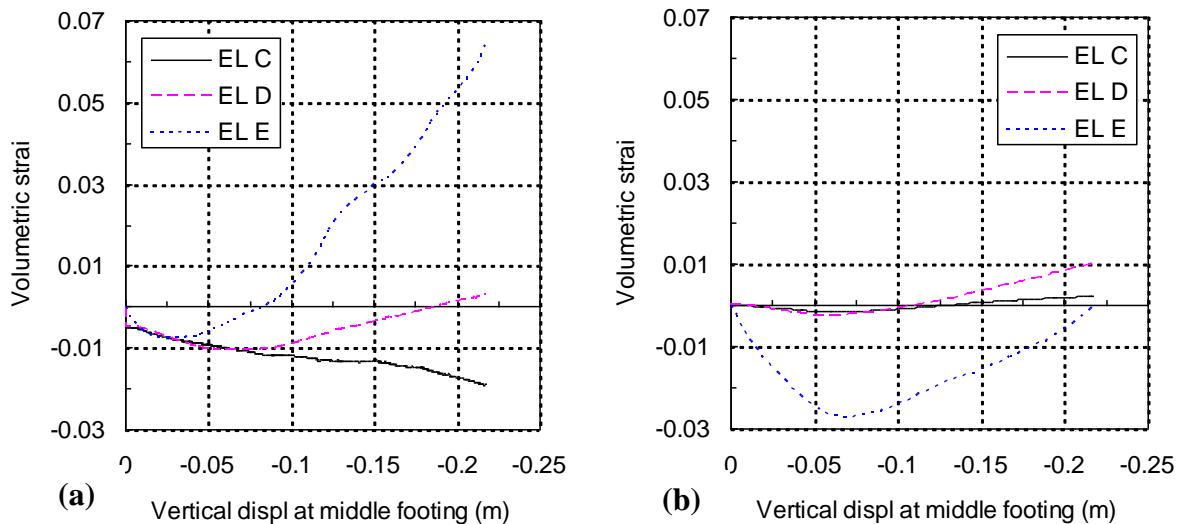


Fig. 31 Evolution of volumetric strain at elements EL C, D, and E by using hypoplastic model, (b) elasto-plastic Drucker Prager model

5. Conclusion

The simulations of oedometric compression, plane strain compression test, and penetration of footing into sand specimen are conducted by using hypoplastic model by Wu Wei (1992). The modification of stress update algorithm is introduced and used in those simulations. The inclusion of this modified algorithm shows an advantage in the sense of convergence especially for oedometric compression and plane strain compression tests. For the single element test, the simulation of oedometric and plane strain compression test using modified version can show homogeneous deformation for arbitrary loading/unloading condition. Homogeneous deformation is also shown when oedometric compression is simulated by using discrete structure while the inhomogeneous deformation is observed in plane strain compression test. This inhomogeneity is due to the material behavior and not due to geometrically reason. The penetration of footing foundation into sand specimen is simulated by using hypoplastic model with modified algorithm and elasto-plastic Drucker Prager model. Both models can capture a tendency of heaving at the certain distance from footing corner. The elasto-plastic Drucker Prager model shows slightly different degree of dilatancy angle at the element closed to the corner of footing. For the element below footing, the elastic-plastic Drucker Prager model shows twice higher degree of compression than that of hypoplastic model. The hypoplastic model can produce similar dilatancy behavior of the soil around the footing to those shown in Prandtl mechanism.

6. References

- Bazant, Z.P., Cedolin, L., 2003, *Stability of Structures: Elastic, Inelastic, Fracture and Damage Theories*, Dover Publication, New York.
- de Borst, R., 1986, *Non-Linear Analysis of Frictional Materials*, Ph.D. Thesis TU-Delft.
- Kolymbas, D., 1991, An Outline of hypoplasticity, *Arch. of Applied Mechanics*, 61, 143-151.
- Kolymbas, D., Wu, W., 1993, Introduction to hypoplasticity, in *Modern Approached to Plasticity*, ed. D. Kolymbas, Elsevier, pp. 213-223.
- Niemunis, A., 1993, Hypoplasticity vs elastoplasticity, selected topics, in *Modern Approached to Plasticity*, ed. D. Kolymbas, Elsevier, pp. 277-307.
- Wu, W., Bauer, E., 1994, A Simple Hypoplastic constitutive model by sand, *Int. J. Numerical and Analytical Methods Geomechanics*, 18, pp. 833-862.